BMC Oral Health

RESEARCH

Open Access

Biomechanical performance of post-and-cores of polyetheretherketone and its composites

Biyao Wang[1], Minghao Huang[2], Kaige Zhang[2], Yan Xu[3], Xinwen Zhang[2,4], Liye Shi[5*†] and Xu Yan[1*†]

Abstract

Background Polyetheretherketone (PEEK) and its fiber-reinforced composites have been indicated as ideal post-and-cores materials due to its mechanical properties. However, the laboratory evidences of post-and-cores restored with fiber-reinforced PEEK are lacking.

Materials and methods A total of 120 extracted mandibular premolars were treated endodontically and divided into six groups restored with different post-and-core materials ($N=20$): (1) prefabricated quartz fiber-reinforced composite (QFRC), (2) polymer-infiltrated ceramic (PIC), (3) cobalt chromium (CoCr), (4) PEEK, (5) 30% glass fiber-reinforced PEEK (GFR-PEEK), and (6) 30% carbon fiber-reinforced PEEK (CFR-PEEK). Stress distribution was analyzed by finite element analysis (FEA). Then, each group was then divided into two subgroups ($n=10$): static loading test and fatigue loading test. The static failure load (SFL) was analyzed by one-way analysis of variance (ANOVA) with least-significant difference (LSD) multiple comparison tests. The fatigue failure load (FFL) and cycles for failure (CFF) were evaluated by Kaplan-Meier survival analysis ($P<0.05$).

Results Groups PEEK, GFR-PEEK, and CFR-PEEK exhibited lower maximum peak principal stress and better stress distribution than Group CoCr. The SFL of Groups PEEK and QFRC did not differ from each other, and both were lower than those of Groups CoCr, GFR-PEEK, and CFR-PEEK. In the fatigue loading test, Group CoCr exhibited the best survival; however, with the progression of fatigue, the survival probabilities of Groups PEEK and its composites were close to that of Group CoCr. In all groups apart from Group CoCr, the rate of repairable failure modes was higher than that of irreparable ones.

Conclusions Customized post-and-cores manufactured with PEEK and its fiber-reinforced composites showed superior biomechanical performance, making them potential alternatives for the restoration of massive tooth defects.

Clinical relevance This study provides a theoretical basis for clinicians to select post-and-core materials for different root canal morphology residual roots and helps to reduce the occurrence of complications such as root fracture and post core debonding.

Keywords Post-and-core, Dental material, Esthetic dentistry, Polymer, Polyetheretherketone

†Liye Shi and Xu Yan contributed equally to this work.

*Correspondence:
Liye Shi
lyshi@cmu.edu.cn
Xu Yan
xyan@cmu.edu.cn

Full list of author information is available at the end of the article

Introduction

The post-and-core material should have high flexural strength, accurate matching with the root canal morphology, sufficient fatigue resistance, and an elastic modulus close to that of dentin (18.6 GPa) [1], in order to form a favorable stress distribution in dentin [2]. It has been demonstrated that the stress distribution is affected by various materials of post-and-cores, which further influence the fracture resistance of the root [3]. The elastic modulus of metal post-and-cores is far higher than that of dentin, resulting in an inhomogeneous stress distribution, which can subsequently lead to root fracture [4]. Cast post-and-cores are custom-made according to the morphology of the root canal, which have the advantages of good adaptation and no need for excessive root canal shaping to accommodate the post. The major disadvantages of cast post-and-cores are their susceptibility to catastrophic root fracture and their unesthetic color. In contrast, the elastic modulus of fiber-reinforced composite (FRC) posts is close to that of dentin, forming a homogeneous stress distribution, which reduces the incidence of root fracture [5]. Currently, quartz fiber-reinforced composite (QFRC) posts are the first choice for clinicians in terms of post-and-core restoration, but they still have some shortcomings. For example, the morphology of these prefabricated posts fails to match various root canals, so a special calibrated drill is required to prepare the post space. Meanwhile, more root dentin needs to be removed and a thicker layer of luting cement must be used, increasing the susceptibility to root fracture and debonding of the FRC posts [6]. There is thus a need to study the stress distribution and fracture resistance of various novel post-and-core materials in the root, in order to find the optimal material for protecting the residual root from refracture.

Polyetheretherketone (PEEK), a semi-crystalline organic polymer compound, has superior mechanical strength, high chemical and thermal resistance, low water solubility, and excellent biocompatibility, and has thus become a hotspot of recent biomedical research [7]. PEEK has a toothcolored appearance and low elastic modulus (3–4 GPa) which is much lower than those of metal and ceramic [7]. The elastic modulus of 30% glass fiber-reinforced PEEK (GFR-PEEK) can reach 12 GPa and that of 30% carbon fiber-reinforced PEEK (CFR-PEEK) can reach 18 GPa, which are even closer to that of human dentin. Meanwhile, the mechanical strength of the fiber-reinforced PEEK composites is also elevated [8]. Post-and-cores made of PEEK and its composites and manufactured using CAD/CAM (Computer-Aided Design/Computer-Aided Manufacture) make up for the shortcomings of prefabricated FRC posts, better matching the morphology of various root canals [9].

Recently, it has been demonstrated that customized PEEK post-and-cores could withstand the occlusal force of normal humans under a static loading test [6, 8, 9] and a conventional fatigue loading test under a loading amplitude of 50 N [10, 11]. Although PEEK post-and-cores exhibited a more favorable stress distribution and failure mode (post debonding) than metal post-and-cores [1], the fracture resistance of PEEK post-and-cores was significantly lower than that of metal post-and-cores [10, 11]. Thus, in this study, GFR-PEEK and CFR-PEEK post-and-cores were compared with conventional post-and-cores in vitro and finite element analysis was used to investigate whether fiber reinforcement could improve the biomechanical performance of PEEK post-and-cores.

Materials and methods

Finite element analysis

This study was conducted in accordance with the Declaration of Helsinki, and the protocol was approved by the Medical Ethics Committee of the Hospital of Stomatology of China Medical University (2022; No. 7). A cone-beam computed tomography (CBCT) scan was performed on a lower second premolar tooth extracted for orthodontic purposes. The scan utilized a voltage of 69 kV and an X-ray beam current of approximately 100 mA, and achieved a resolution of 20 μm. The resulting images were saved in Digital Imaging and Communications in Medicine (DICOM) format. To create the surface model, the scanned data were imported into the 3D image processing program Mimics Medical 21.0 (Materialise Medical, Leuven, Belgium) and Geomagic Wrap 2017 (Geomagic Inc., Salt Lake City, UT, USA) to reconstruct a premolar tooth model. Furthermore, the CAD software Solidworks 2018 (Waltham, MA, USA) was applied to section the model 2 mm above the enamel-osseous junction, which was used to obtain a model of the post-and-core crown with complete dentin ferrule. The model was then assembled in the software, which consisted of all of the cortical bone, cancellous bone, periodontal ligament, dentin, post-core, crown cement, and post-core cement (Fig. 1A). The model was further classified according to the different post-core materials, as mentioned above.

The finite element analysis software ANSYS Workbench 2021 R1 (Swanson Analysis, Canonsburg, PA, USA) was applied for meshing and biomechanical analysis of the models. The assemblies were meshed with 1,405,312–1,411,849 elements and 1,995,631–2,009,268 nodes, and the orthogonal quality ranged from 0.8523 to 0.8571, as determined by mesh sensitivity analysis. Some of the data on modulus of elasticity and Poisson's ratio were obtained from the manufacturer and others were from reports in well-respected journals (Table 1). In the idealized simulation, all components are designated as homogeneous, isotropic, linear elastic materials. All

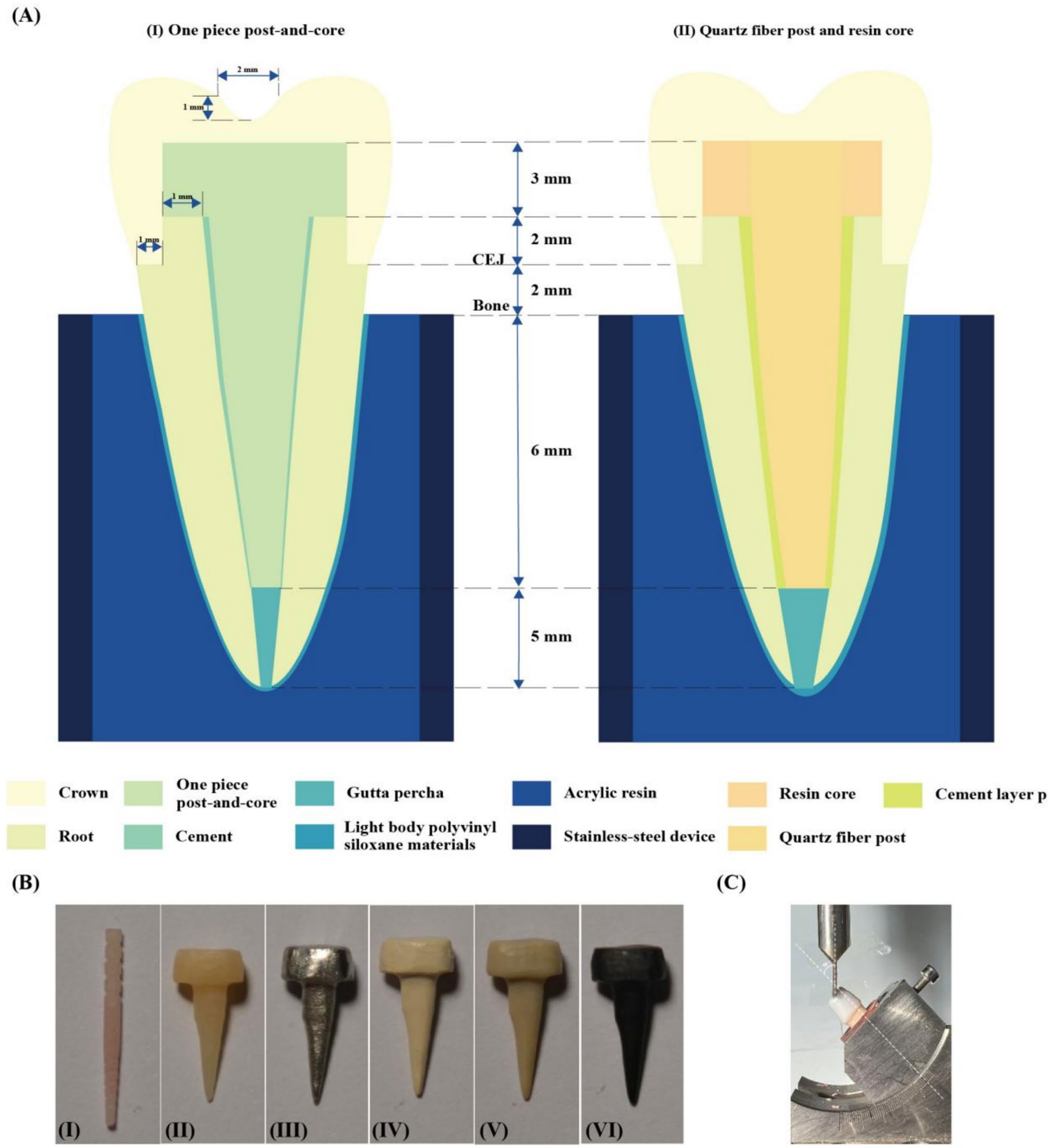

Fig. 1 Specimen preparation and specimen on testing machine. (**A**) Schematic illustration and the dimensions of the post-and-core and crown (mm). (**B**) Different post-and-cores. (**B-I**) QFRC post. **(B-II)** PIC post-and-core. **(B-III)** CoCr post-and-core. **(B-IV)** PEEK post-and-core. (**B-V**) GFR-PEEK post-and-core. **(B-VI)** GFR-PEEK post-and-core. (**C**) The specimen was set in the fatigue testing machine

model interfaces are specified with bonded contact, and the cortical bone surface is assumed to be rigidly fixed in the x, y, and z directions. A static occlusal force of 180 N is applied to the buccal apical lingual bevel of the crown at an angle of 45° to the longitudinal axis of the tooth, 2 mm below the cusp [12, 13]. In this study, owing to the inherent brittleness of dentin and other post-core materials, the maximum principal stress was employed to analyze the results based on the Rankine criteria for dentin failure [14]. For each group of dental model components,

Table 1 Physical properties of the materials used [15]

Material	Elastic modulus (GPa)	Poisson's coefficient
Cortical bone	13.7	0.3
Spongy bone	1.37	0.3
Periodontal ligament	0.069	0.45
Dentin	18.6	0.31
Gutta-percha	0.00069	0.45
Resin cement	18.6	0.28
Glass ionomer cement	4	0.35
Resin core	12	0.3
Quartz-fiber-reinforced composite (QFRC)	32.1	0.3
Polymerized porcelain (PIC)	10.3	0.3
Cobalt chromium alloy (CoCr)	200	0.42
Polyetheretherketone (PEEK)	4.5	0.17
30% Glass fiber-reinforced PEEK (GFR-PEEK)	12	0.4
30% Carbon fiber-reinforced PEEK (CFR-PEEK)	18	0.39
Zirconia crown	210	0.3

the stress distribution outcomes were visualized using contour plots. The color scale within these plots represents pressure in megapascals (MPa), facilitating comparisons between the analyzed models.

Specimen preparation

A total of 120 single-rooted premolars were selected in line with the inclusion and exclusion criteria listed below. They were healthy teeth recently extracted (within 6 weeks of extraction) for orthodontic reasons and the informed consents have been obtained from the patients. The buccolingual and mesiodistal diameters of the coronal planes were measured using digital caliper (DELIXI, Zhejiang, China). The inclusion criteria were as follows: mesiodistal width of between 4.50 and 6.00 mm measured at 14.00 mm from the root apex, buccolingual width of between 6.50 and 8.50 mm measured at 14.00 mm from the root apex, and root length of between 14.00 and 16.00 mm measured from the root apex to the CEJ. The canal morphology of each tooth was verified using periapical radiographs in both mesio-distal and bucco-lingual directions. The exclusion criteria were as follows: teeth with crown destruction as a result of decay or trauma, cracks or fracture lines in crowns or roots, no overlapping crown–root line, or unsuitable diameter or length for the study.

The specimens were randomly assigned to six experimental groups using a computer-generated list ($N = 20$), according to the material used to manufacture the post-and-core: Group 1, QFRC post and composite core; Group 2, polymer-infiltrated ceramic (PIC) post-and-core; Group 3, CoCr post-and-core; Group 4, PEEK post-and-core; Group 5, 30% GFR-PEEK post-and-core; and Group 6, 30% CFR-PEEK post-and-core. Each group was subsequently divided into two subgroups ($n = 10$): static loading group and fatigue loading group. The components and mechanical properties of the different post-and-core materials are shown in Table 2.

All preparation steps were performed by one of the researchers to avoid inter-operator variation. The coronal portion was sectioned 2.00 mm above the cemento-enamel junction (CEJ) by using a round bur (Mani, Japan) with a high-speed handpiece; therefore, the specimen was about 15.00 mm long with a 1.00 mm-wide shoulder, as shown in Fig. 1A. The entrance of the root canal was widened, leaving a ferrule 1.00 mm thick and 2.00 mm high. The working length was established at 1.00 mm from the apex by introducing a number 10 K-file (Dentsply Maillefer, Ballaigues, Switzerland) to confirm root canal permeability. Biomechanical preparation was performed at the working length with hand files (Protaper Universal System; Dentsply Maillefer) and rotary instrumentation (X-smart Plus; Dentsply Maillefer) up to the F3 file. The root canal was irrigated with 0.3% sodium hypochlorite (Feng Yuan Pharmaceutical, Anhui, China) and 18% ethylenediaminetetraacetic acid (Fengyuan Pharmaceutical, Anhui, China) for 30 s after each instrument change, and the root canal was subsequently washed with water. Then, the root canal was air-dried and dried with paper points. AH-Plus sealer (Dentsply DeTrey GmbH, Konstanz, Germany) and F3 gutta-percha master cone (Dentsply Maillefer) were used to fill the root canal. A hydraulic

Table 2 The components and mechanical properties of the different post-and-core materials

Material	Commercial Name	Manufacturer	Matrix and Filler (weight%)	Elastic Modulus (GPa)	Flexural Strength (MPa)
Dentin	-	-	-	18.6	212.9
QFRC	MACRO-LOCK®POST ILLUSION®X-RO®	RTD, St-Egreve, France	80% quartz fiber and 20% epoxy resin	32.1	-
PIC	BRILLIANT Crios	Coltene, Germany	70.7% nano-ceramic and 29.3% resin matrix	10.3	262
CoCr	Wirobond C+	BEGO, Germany	63.9% Co, 24.7% Cr, 5.4% W, 5% Mo, and 1% Si	200	650
PEEK	BioPAEK	DENTEX, Jinlin, China	PEEK filled with 5%TiO_2 and tiny amounts of Fe_2O_3	4.5	180–190
GFR-PEEK	JUTAIPEEK GF30G	Jutai, Suzhou, China	PEEK filled with 30% glass fiber	12	200
CFR-PEEK	JUTAIPEEK CF30G	Jutai, Suzhou, China	PEEK filled with 30% carbon fiber	18	195

temporary restorative material, CAVITON (Erzhi Dentistry, Suzhou, China), was used to fill the access cavity, which is mainly composed of zinc oxide, calcium sulfate, polyvinyl acetate composition. The teeth were stored at 37 °C and 100% relative humidity.

To imitate the physical condition of the root, light body polyvinyl siloxane materials (Dentsply Maillefer) were used to simulate the periodontal ligament. Twenty-four hours after the root was endodontically treated, it was initially dipped into melted wax up to 2.00 mm below CEJ with a thickness of 0.20–0.30 mm. The root was later embedded in a custom silicone mold (15.00 mm high and 16.00 mm in diameter; Chenyang Silicone Technology, Shenzhen, China) with acrylic resin (Juhengchuang Electronic Materials, Shenzhen, China). The root was arranged parallel to the vertical axis of the silicone mold by using a surveyor and the upper surface of the acrylic resin and silicone mold were 2 mm below the CEJ to imitate the alveolar bone level. After 24 h, the wax was removed and the root was covered with light body and embedded again into the prepared sockets.

In Groups PIC, CoCr, PEEK, GFR-PEEK, and CFR-PEEK, one-piece post-and-cores were shown in Fig. 1A-I. The temporary restorative material was removed and then the root canal was prepared with number 1 and 2 Peeso burs (Mani, Tokyo, Japan) to a depth of 10.00 mm. The post space length for all samples was set at approximately 10.00 mm with the help of silicone stoppers. The impression of the post space was obtained by using the light body polyvinyl siloxane materials (Dentsply Maillefer) for PIC, CoCr, PEEK, GFR-PEEK, and CFR-PEEK post-and-cores. The digital impression was obtained using a lab scanner (3D Scanner AutoScan-DS-EX; Shining 3D, Hangzhou, China) and it was milled in a milling machine (Dental Cutting Machine-AM-X5; Aidite, Qinhuangdao, China). In terms of the post-and-core dimensions, the design conferred a 2.5% smaller volume for cementation and the height of the core was designed to be 3.00 mm using CAD/CAM software (exoCAD Dental; exoCAD GmbH, Darmstadt, Germany). The post-and-core was tried into each tooth and the root canal was dried with paper points. All of the post-and-cores used in this study are shown in Fig. 1B.

Each finished post-and-core was cleaned with 75% alcohol, air-dried, and then underwent surface treatment as per the manufacturer's instructions. The CoCr (Wirobond C+; BEGO Bremer Goldschlagerei Wilh. Herbst GmbH & Co. KG, Warren, Germany) post-and-core surface was preconditioned with 110 µm aluminum oxide sandblasting (Cobra; Renfert GmbH, Hilzingen, Germany) for 15 s at a distance of 10.00 mm under 3.5 bar pressure and subsequently rinsed with water. The post canal was filled with glass ionomer cement (HY-BOND GLASIONOMER CX; Shofu, Kyoto, Japan) with no preconditioning of the radicular dentin. The mixing ratio of the powder and liquid was 2:1 and the mixing time was 30 s. The post was placed within the canal and held in position with moderate finger pressure for 3 min. The excess cement was removed with a cotton pellet. PIC (BRILLIANT Crios; Coltene, Altstätten, Switzerland) post-and-core surface was preconditioned with 50 µm aluminum oxide sandblasting (Cobra; Renfert GmbH) for 15 s at a distance of 10.00 mm under 2 bar pressure and subsequently rinsed with water. A universal primer (ONE COAT 7 UNIVERSAL; Coltene) was applied to the post surface for 20 s, followed by air-drying for 5 s and then light-curing for 30 s with an LED light curing unit (SERVOTOME, France). PEEK (BioPAEK; DENTEX, Jilin, China), GFR-PEEK (Jutai, Suzhou, China), and CFR-PEEK (Jutai, Suzhou, China) post-and-core surfaces were preconditioned with 110 µm aluminum oxide sandblasting (Cobra; Renfert GmbH) for 15 s at a distance of 10.00 mm under 3.5 bar pressure and were subsequently rinsed with water. A bonding primer (Visio.link; Bredent GmbH, Senden, Germany) was coated on the PEEK surface, air-dried for 20 s, and then light-cured for 90 s.

PIC, PEEK, GFR-PEEK, and CFR-PEEK post-and-cores were cemented with self-adhesive resin luting cement (RelyX U200; 3 M ESPE, Seefeld, Germany). The post space was filled with self-adhesive resin cement. The post was placed within the space and held in position with moderate finger pressure. The excess cement was removed with a cotton pellet. Each specimen was light-cured for 20 s from four directions. The abutment tooth was prepared with a height of 5.00 mm and a 1.00 mm-wide shoulder by using a round bur (Mani, Japan) with a high-speed handpiece, as shown in Fig. 1A-I.

In Group QFRC, the temporary restorative material was removed and then the root canal was prepared with number 1 and 2 Peeso burs (Mani, Japan) to a depth of 10.00 mm with the help of silicone stoppers. The post space of the prefabricated post was refined with a number 2 post finishing drill (RTD, St-Egreve, France). The canal was etched with 37% phosphoric acid (DX. Etch 37; DENTEX, Jilin, China) for 15 s, rinsed, and dried with paper points. A bonding agent (SE ONE; Kuraray Noritake Dental, Tokyo, Japan) was applied to the root canal walls, air-dried for 10 s, and then light-cured for 10 s. The QFRC post was cleaned with 75% alcohol and then air-dried. An abutment was built up via a direct method using the number 2 QFRC post (MACRO-LOCK®POST ILLUSION®X-RO®; RTD, St-Egreve, France) and resin composite (DC Core ONE; Kuraray Noritake Dental, Tokyo, Japan). The abutment was 3.00 mm above the ferrule. Each specimen was light-cured for 40 s from five directions. The abutment tooth was prepared with a height of 5.00 mm and a 1.00 mm-wide shoulder by using a round bur (Mani, Japan) with a high-speed handpiece, as shown in Fig. 1A-II.

A digital impression of the abutment tooth was obtained by using a lab scanner (3D Scanner AutoScan-DS-EX; Shining 3D, Hangzhou, China) and it was milled in a milling machine (Dental Cutting Machine-AM-X5; Aidite, Qinhuangdao, China). The zirconia crown (QGW9814190404182; Aidite, Qinhuangdao, China) was designed for bicuspid mandibular premolars with a thickness of 0.5 mm in each section and a circular notch (2.00 mm in diameter and 1.00 mm deep) at the central groove for load application by using CAD software (exoCAD Dental; exoCAD GmbH, Darmstadt, Germany), as shown in Fig. 1A. All procedures of crown manufacturing were performed by a dental technician who had received training in such manufacturing. Each crown was tried in each tooth and air-dried. Self-adhesive resin cement (RelyX U200; 3 M ESPE, Seefeld, Germany) was used for crown adhesion. Each specimen was light-cured for 20 s from four directions. The specimens were stored at 37 °C and 100% relative humidity.

Thermocycling

All specimens were stored at 100% humidity for 24 h. They were then subjected to thermocycling (1100; SD Mechatronik, Germany) for 5000 thermal cycles (5 °C/55°C; dwell time, 20 s), which corresponds to approximately 4 to 5 years of clinical service [16, 17].

Static loading test

After thermocycling, half of the specimens from each group were subjected to a compressive load using an electromagnetic force fatigue testing machine (M-12000; CARE Measurement & Control, Tianjin, China) with a crosshead speed of 0.50 mm/min. A stainless-steel indenter with a 1.00 mm-diameter hemisphere cusp was used. The indenter tip was applied on the prepared circular notch at the lingual incline plane of the buccal cusp of the crown to standardize the load direction and avoid slipping. To control the angle of the loading, a stainless-steel metal device containing a hole, which had an axis of 45 in relation to the loading axis, was used (Fig. 1C). Loading was performed until fracture occurred, detected by a sudden drop of the load. The static failure load (SFL, in Newtons) and the failure mode were recorded.

Fatigue loading test

The other specimens of each group were subjected to testing in an electromagnetic force fatigue testing machine (M-12000; CARE Measurement & Control, Tianjin, China). The same indenter and the stainless-steel metal device were used the same as in the static loading test to standardize load direction and avoid slipping. A stepped-load cyclic fatigue test was used to evaluate the fatigue resistance of different post-and-core materials [18]. The loading cycles were sinusoidal at 5 Hz [18]. The maximum load increased with time and the minimum load for each cycle was 10% of the maximum load [18]. A warm-up load of 5×10^3 cycles was performed at the load range from 10 to 100 N [18]. Then, the maximum load was applied in the range from 200 to 1000 N, each for 1.5×10^4 cycles (Table 3) [18]. Samples were loaded until failure or to a maximum of 1.4 million cycles at 1000 N [18]. The fatigue failure load (FFL), failure mode, and cycles for failure (CFF) were recorded [18].

Fracture pattern analysis

When the test ended, the specimens were extracted from the acrylic resin and the failure mode was recorded by a digital camera (D3100; Nikon, Thailand). The failure patterns were categorized into six types in accordance with the fracture location (with 1–3 reflecting repairable failure and 4–6 reflecting irreparable failure) [19, 20]: 1 = crown or core fracture; 2 = post debonding; 3 = root fracture in the cervical third (fracture extending within 1/3 the length of the root, longitudinally from the cervical portion); 4 = root fracture in the middle third (fracture extending between 1/3 and 2/3 from the cervical to apical portion); 5 = root fracture in the apical third (fracture extending longitudinally to the apical third of the root); and 6 = vertical root fracture.

Statistics

The distributions of the static failure load of different post-and-core materials were assessed using the Shapiro-Wilk method. The Shapiro-Wilk test for normality ($P = 0.200$) and Levene test for homogeneity ($P = 0.275$) revealed that the static failure load data of the specimens were normally distributed. Then, considering that the static failure load variable was also normally distributed in the subgroups, the mean and standard deviation along with 95% confidence interval were used to describe the distribution. The static failure load was analyzed using one-way analysis of variance (ANOVA) with least-significant difference (LSD) multiple comparison tests. The Kaplan-Meier test was used to compare the fatigue failure load (FFL) and cycles for failure (CFL) among different post-and-core materials, followed by the post

Table 3 Loading amplitudes and corresponding numbers of cycles for accelerated fatigue test

Step	1	2	3	4	5	6	7	8	9	10
Loading amplitude (N)	100	200	300	400	500	600	700	800	900	1000
Number of cycles	5×10^3	1.5×10^4	1.5×10^4	1.5×10^4	1.5×10^4	1.5×10^4	1.5×10^4	1.5×10^4	1.5×10^4	1.5×10^4

hoc log-rank test. Differences between fatigue failure load and static failure load within each group were analyzed by Student's t-test. A series of χ^2 tests and Bonferroni adjustments were used to compare the incidence of irreparable failure among the groups in the static loading test and fatigue loading test, respectively. The observed significance level (*P*-value) for the χ^2 tests was computed by the Pearson chi-squared test. These approaches lead to valid conclusions even in cases where the methodological assumptions of the χ^2 test are not fulfilled. Statistical analyses were conducted using SPSS version 24 (SPSS Inc; Chicago, United States), and *P*-values of < 0.05 were considered statistically significant.

Results

Finite element analysis

Figure 2A shows the maximum peak principal stress in the post-core, dentin, and cement p for each group of models. In terms of roots, there was no obvious difference in the maximum peak principal stress on dentin among the different post-core materials; the largest stress value was found in Group PEEK and the smallest in Group CoCr. For post-and-cores, Group CoCr exhibited the highest stress value, followed by Groups QFRC, CFR-PEEK, GFR-PEEK, PIC, and PEEK. In terms of bonding, the adhesive cement stress was highest for bonding QFRC, while the peak maximum principal stress values for PIC, PEEK, GFR-PEEK, and CFR-PEEK were close to each other, whereas that of CoCr was significantly lower.

Figure 2B shows the maximum principal stress distribution in six groups. For dentin, the maximum peak principal stress was concentrated at the junction of the lingual side of the root with the alveolar bone in all groups. For post-and-cores, the distribution of maximum principal stress in each group was significantly different. In Group CoCr, the stress was concentrated in the middle third of the post. In Groups PIC and PEEK, the stress was concentrated in the cervical third of the post, whereas in Groups QFRC, GFR-PEEK, and CFR-PEEK, the stress distribution was more uniform, being mainly concentrated in the cervical third of the post and partly concentrated in the lower part of the middle third of the post. The location of the maximum principal stress in the cement layer p was similar but not identical to that of the post-core in all groups. This was mainly due to the fact that the stress in PIC, PEEK, GFR-PEEK, and CFR-PEEK was not entirely concentrated lingually, but rather proximally and distally at the interface of the post and dentin junction.

Static loading test

The static failure loads (mean ± SD, N) of different post-and-cores were 305.46 ± 45.57 (QFRC), 452.24 ± 106.69 (PIC), 532.78 ± 40.35 (CoCr), 372.03 ± 66.96 (PEEK), 481.84 ± 79.22 (GFR-PEEK), and 471.82 ± 86.83 (CFR-PEEK) (Fig. 3A), which differed significantly ($P < 0.001$). No significant difference was found between the PEEK and QFRC groups, and both of their values were lower than those in the other groups. Group GFR-PEEK did not differ from Group CFR-PEEK and both had significantly higher values than Group PEEK. There was no significant difference between Groups GFR-PEEK and PIC, nor between Groups CFR-PEEK and CoCr.

Figure 3B illustrates the rates of different failure modes observed in different post-and-cores. The rates of irreparable failure mode in the static loading test were as follows: QFRC (0%), PIC (10%), CoCr (80%), PEEK (0%), GFR-PEEK (10%), and CFR-PEEK (20%). In Groups PEEK, GFR-PEEK, CFR-PEEK, QFRC, and PIC, the rate of repairable failure modes was higher than that of irreparable ones, while in Group CoCr the opposite pattern was shown. CoCr post-and-cores showed a higher incidence of irreparable failures than the other groups, while there was no significant difference in this regard among the other groups. The representative static failure modes of each material are shown in Fig. 3C.

Fatigue loading test

All specimens failed before the end of the fatigue loading test (140 000 cycles). Table 4 shows the survival probability through the progression of the fatigue test with increasing loading, which combines the results of fatigue failure load and cycles for failure.

The fatigue resistance survival curves in terms of fatigue cycles are presented for all 60 specimens (Fig. 4A). The numbers of cycles until initial failure for Groups QFRC, PIC, and PEEK were between 5 500 and 6 000, while for Groups CoCr, GFR-PEEK, and CFR-PEEK they were between 18 000 and 21 000. CoCr post-and-cores almost always exhibited the best survival among these materials. However, with the progression of fatigue, the survival probabilities of Groups PEEK, GFR-PEEK, and CFR-PEEK approached that of Group CoCr. Groups QFRC and PIC always had lower survival than the other groups. The longest survival time was shown in Group CFR-PEEK (50 000 cycles), while the shortest was shown in Groups QFRC and PIC (35 000 cycles). The survival time for Groups CoCr, PEEK, and GFR-PEEK was between 40 000 and 42 000 cycles.

The numbers of cycles for failure (mean ± SD) of different post-and-cores were as follows: 19327.60 ± 2620.08 (QFRC), 18492.70 ± 3623.29 (PIC), 28631.90 ± 2912.10 (CoCr), 24329.10 ± 3686.85 (PEEK), 27367.80 ± 2986.82 (GFR-PEEK), and 29018.50 ± 3674.79 (CFR-PEEK) (Fig. 4B). The Kaplan-Meier survival test identified a significant difference among the groups regarding the number of cycles for failure ($P < 0.05$). The mean number of cycles for failure of Group CoCr was significantly higher

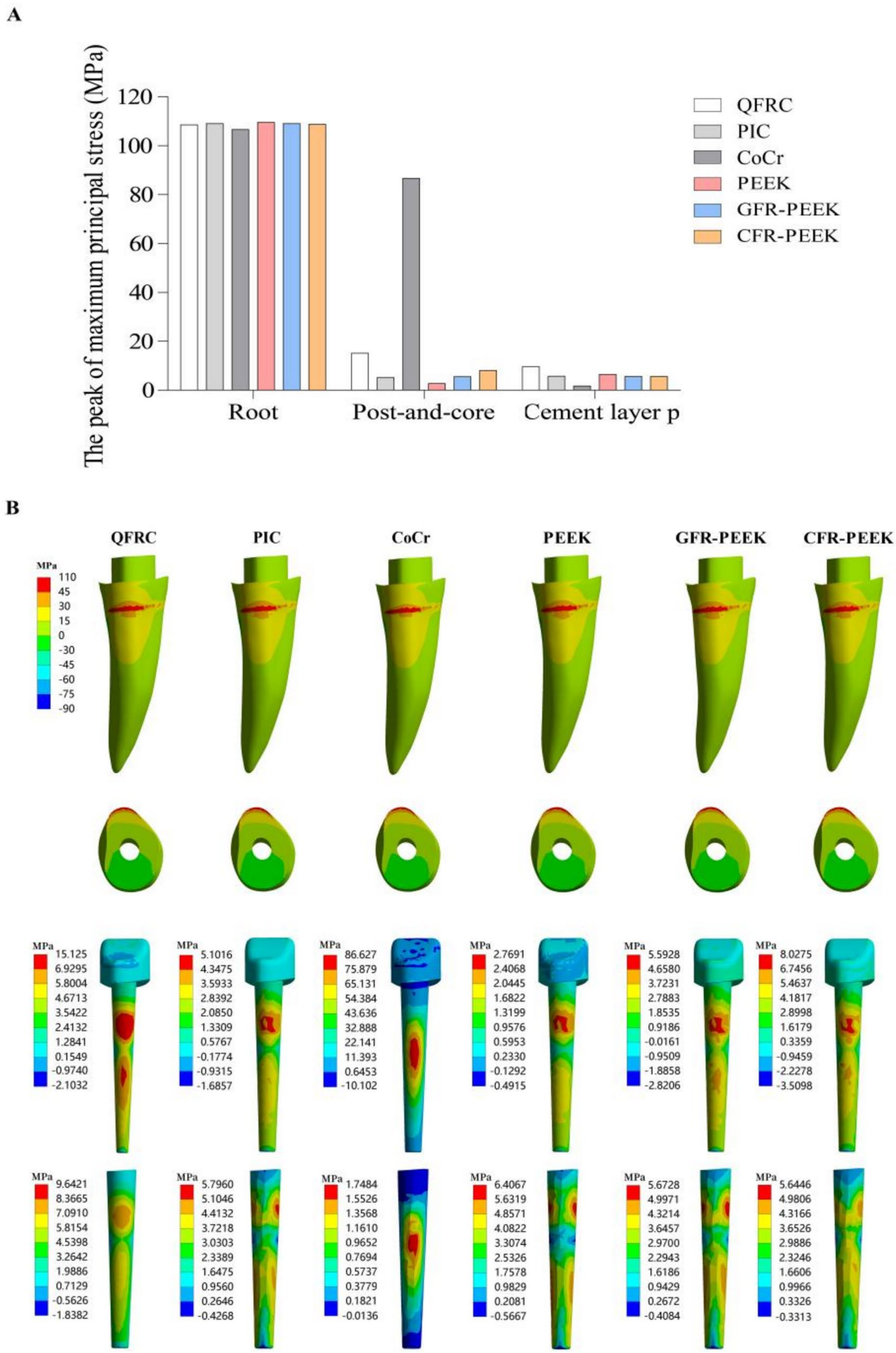

Fig. 2 Finite element analysis. (**A**) Peak maximum principal stress in Group 1 to Group 6 with restored tooth components: root, post-core, and cement layer p. (**B**) Distribution of maximum principal stress in each group within restored tooth components: root, post-core, and cement layer p

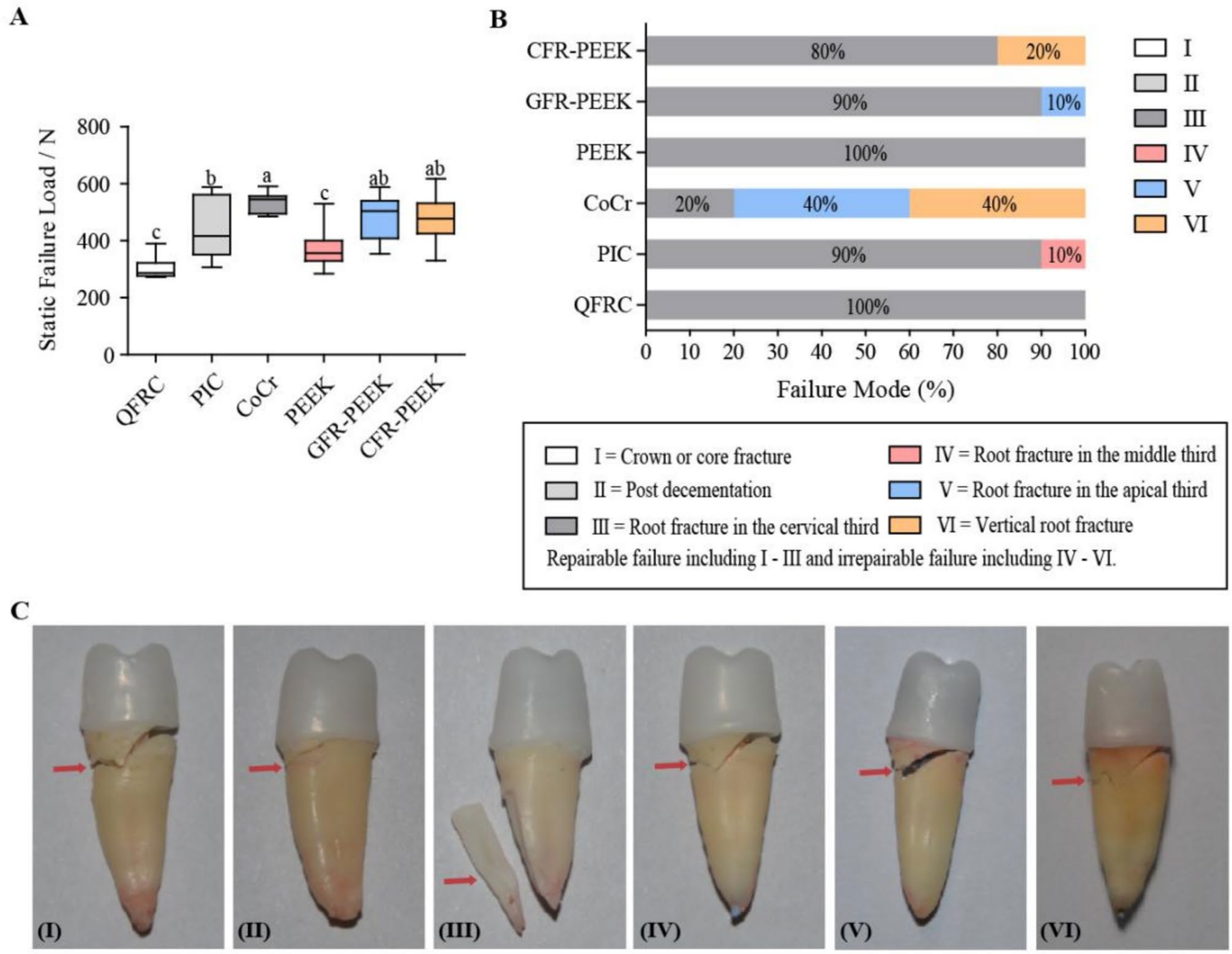

Fig. 3 Static loading test. (**A**) Static failure load of different post-and-cores [different lower-case letters indicate significant differences, $P < 0.05$; one-way analysis of variance (ANOVA) with least-significant difference (LSD) multiple comparison tests]. Box-and-whisker diagram of static failure loads presenting the median (bold black horizontal line), minimum and maximum values (vertical "t" lines or whiskers) of different post-and-core materials. (**B**) Failure mode analysis of different post-and-core materials regarding the static loading test. (**C**) The representative failure mode of each material in the static loading test; the arrow points out the fracture area. (**C-I**) Root fracture in the cervical third was shown in Group QFRC. **(C-II)** Root fracture in the cervical third was shown in Group PIC, and the fracture line was closer to the crown margin. **(C-III)** Vertical root fracture was shown in Group CoCr. **(C-IV)** Root fracture in the cervical third was shown in Group PEEK. (**C-V**) Root fracture in the cervical third was shown in Group GFR-PEEK. **(C-VI)** Root fracture in the cervical third was shown in Group CFR-PEEK

Table 4 Survival probability (likelihood of specimen exceeding respective load or number of cycles without fracture and respective standard error measurements) for different load steps and numbers of cycles

Groups	Steps of fatigue failure load (*N*) / cycles for failure				
	100 *N* / 5×10^3	200 *N* / 2×10^4	300 *N* / 3.5×10^4	400 *N* / 5×10^4	500 *N* / 6.5×10^4
QFRC	1.00	0.80 (0.13)	0.10 (0.10)	0.00	-
PIC	1.00	0.60 (0.16)	0.10 (0.10)	0.00	-
CoCr	1.00	0.90 (0.10)	0.40 (0.16)	0.00	-
PEEK	1.00	0.80 (0.13)	0.30 (0.15)	0.00	-
GFR-PEEK	1.00	0.80 (0.13)	0.30 (0.15)	0.00	-
CFR-PEEK	1.00	0.90 (0.10)	0.20 (0.13)	0.10 (0.10)	0.00

The sign "-" indicates that no specimens were tested in this step

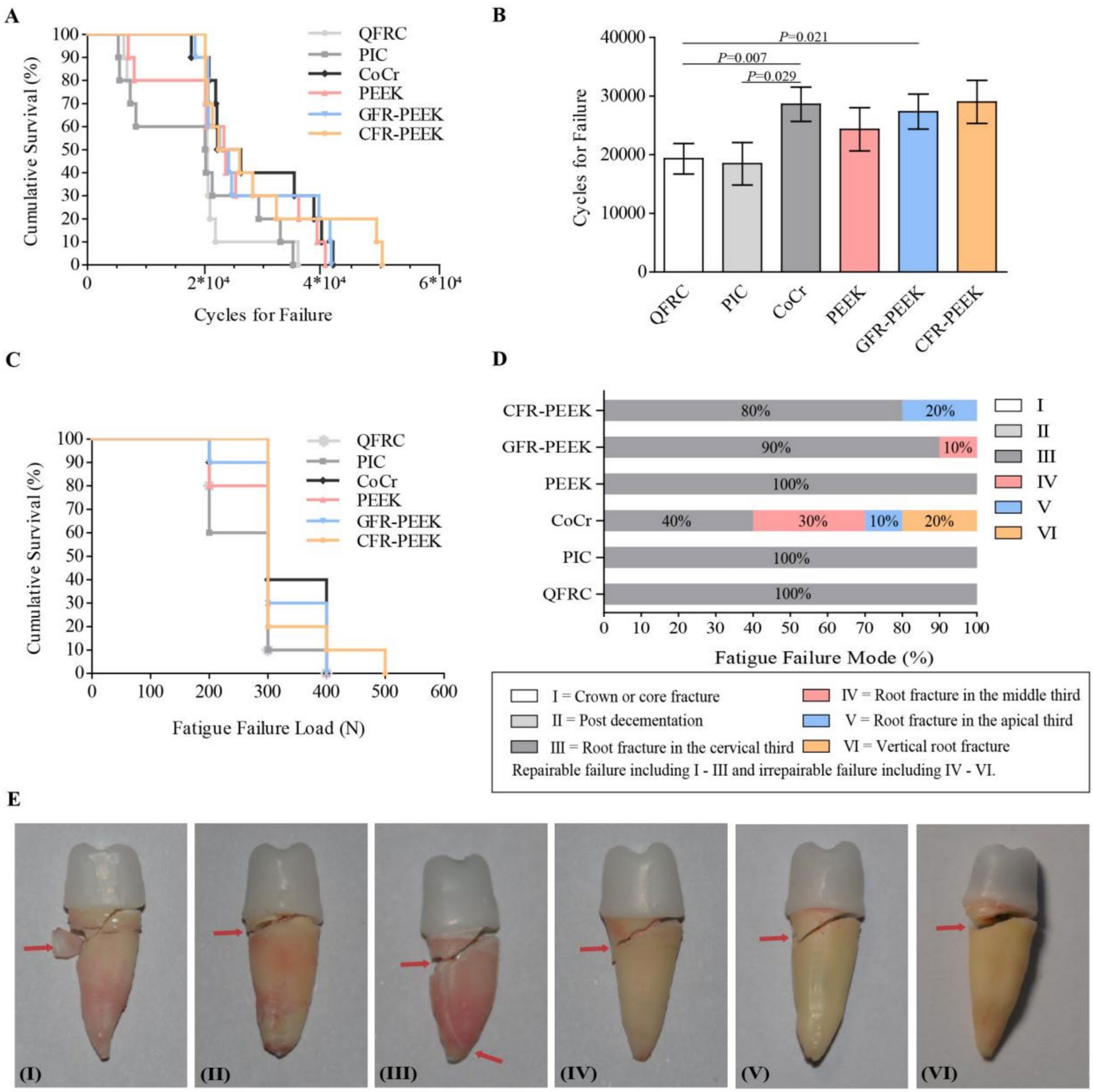

Fig. 4 Fatigue loading test. (**A**) Kaplan-Meier fatigue resistance survival curves in terms of cycles for failure. (**B**) Mean survived cycles and standard errors of cycles for failure ($P < 0.05$, Kaplan-Meier test followed by post hoc log-rank test). (**C**) Kaplan-Meier fatigue resistance survival curves in terms of fatigue failure load. (**D**) Failure mode analysis of different post-and-core materials regarding the fatigue loading test. (**E**) The representative failure mode of each material in the fatigue loading test; the arrow points out the fracture area. (**E-I**) Root fracture in the cervical third was shown in Group QFRC. **(E-II)** Root fracture in the cervical third was shown in Group PIC, and the fracture line was closer to the crown margin. **(E-III)** Vertical root fracture concomitant with cervical-third fracture was shown in Group CoCr. **(E-IV)** Root fracture in the cervical third was shown in Group PEEK. (**E-V**) Root fracture in the cervical third was shown in Group GFR-PEEK. **(E-VI)** Root fracture in the cervical third was shown in Group CFR-PEEK

than those of Groups QFRC and PIC. Group GFR-PEEK showed more cycles than Group QFRC, while there was no statistically significant difference among the other groups.

The fatigue resistance survival curves in terms of fatigue loads are presented for all 60 specimens (Fig. 4C). The highest initial failure load was shown in Group CFR-PEEK (300 N), while the other groups exhibited the same load at 200 N. Group CFR-PEEK almost always exhibited better survival than the other groups before the fatigue load was set at 300 N; however, it had a lower survival probability than Groups CoCr, PEEK, and GFR-PEEK when the load was set between 300 and 400 N. The highest final failure load was observed in Group CFR-PEEK (500 N), while the other groups exhibited the same one at 400 N.

The fatigue failure loads (mean ± SD, N) of different post-and-cores were as follows: 290 ± 17.95 (QFRC), 270 ± 21.34 (PIC), 330 ± 21.34 (CoCr), 310 ± 23.33 (PEEK), 320 ± 20.00 (GFR-PEEK), and 330 ± 21.34 (CFR-PEEK). The Kaplan-Meier survival test identified no significant difference among the groups regarding the fatigue failure load ($P = 0.261$).

Figure 4D illustrates the rates of different failure modes observed in different post-and-cores. The rates of irreparable failure mode in the fatigue loading test were as follows: QFRC (0%), PIC (0%), CoCr (60%), PEEK (0%), GFR-PEEK (10%), and CFR-PEEK (20%). In Group CoCr, the rate of irreparable failure modes was higher than that of repairable ones, while in the other groups the opposite pattern was observed. The χ^2 test identified a significant difference among the groups in terms of fatigue failure mode ($P < 0.01$). No significant differences were found among CoCr, GFR-PEEK, and CFR-PEEK post-and-cores. CoCr post-and-cores showed a higher rate of irreparable failures than the other three groups. There was no statistically significant difference among Groups QFRC, PIC, PEEK, GFR-PEEK, and CFR-PEEK in this regard. The representative fatigue failure modes of each material are shown in Fig. 4E.

Fatigue failure load was significantly lower (by 32–40%) than the corresponding static failure load in Groups PIC, CoCr, GFR-PEEK, and CFR-PEEK ($P < 0.05$). No significant differences were found between the FFL and the SFL in the other groups.

Discussion

PEEK is regarded as a promising alternative to conventional materials for post-and-core restoration due to its excellent mechanical, chemical, and esthetic properties and its biocompatibility. This study investigated the biomechanical performance of post-and-cores of PEEK and its fiber-reinforced composites compared with that of three other post-and-core systems. In the finite element analysis, PEEK and its composites exhibited better stress distribution and lower stress concentration when compared with CoCr, indicating their potential to be applied in post-and-core restoration. Subsequently, the static and fatigue loading tests were carried out.

The bonding strength is known to affect the mechanical behavior of post-and-core systems, so in this in vitro study the whole specimen was conceptualized as a bonded tooth-post-core-crown "monobloc" restoration. An appropriate bonding system was applied for each post-and-core from the following three perspectives: surface modification, primer, and luting cement. PEEK has an inert and poorly adhesive hydrophobic surface. The application of resin-based luting cement alone often fails to provide sufficient bonding strength for PEEK [7]. Sulfuric acid at 98% and sandblasting showed significant improvement of the bonding strength of PEEK posts to resin cement [21, 22]. However, in consideration of chairside safety, we refrained from using sulfuric acid. In this study, sandblasting and a self-adhesive resin cement (RelyX U200, 3 M) [22, 23] were applied to improve the bonding strength of PEEK and its fiber-reinforced composites. Moreover, satisfactory bonding strength can be achieved by Visio.link (Bredent GmbH, Senden, German) because of its specific composition of pentaerythritol triacrylate (PETIA) in solution, methylmethacrylate (MMA) monomers, and additional dimethacrylates, which causes micro-interlocking between resin cement and PEEK and increases the bonding strength of PEEK [24]. For this reason, Visio.link was chosen as a primer in this study.

PEEK has a lower elastic modulus (4.5 GPa) than dentin (18.6 GPa), but similar flexural strength to that of dentin (PEEK: 200 MPa, dentin: 212.9 MPa) [1]. In the FEA of this study, when compared with QFRC and CoCr post-and-cores, a lower stress concentration and better stress distribution were generated in PEEK post-and-cores due to their flexibility, which has also been demonstrated in other studies [1, 10, 25]. GFR-PEEK at 30% and CFR-PEEK at 30% have low elastic moduli (12 and 18 GPa), which are more similar to that of dentin than that of PEEK. In this study, no significant difference was found among Groups PEEK, GFR-PEEK, and CFR-PEEK in terms of peak maximum principal stress, but the values became higher with increasing elastic modulus. In another FEA study, CFR-PEEK was reported to decrease the incidence of post debonding and root vertical fracture, while the strain of CFR-PEEK was the closest to that of dentin [25]. In this study, GFR-PEEK and CFR-PEEK were first used as post-and-cores in static and fatigue loading tests. The static failure loads of PEEK, GFR-PEEK, and CFR-PEEK post-and-cores were higher than the normal occlusal load of an adult, which varies between 200 and 360 N in the posterior region [26]. The present findings are not only in agreement with several previous studies conducted on the mandibular premolars [6, 8, 9], but also similar to those conducted on the anterior teeth [27, 28]. The SFL of Group GFR-PEEK did not differ from that of Group CFR-PEEK and both were significantly higher than that of Group PEEK. The SFL of these two materials were close to that of CoCr, but decreased the incidence of irreparable failure (CoCr 80%) due to their low elastic moduli. The predominant failure mode of Group PEEK was root fracture in the cervical third; meanwhile, the stress was also concentrated in the cervical third, which is consistent with the findings of Haralur et al. and Pourkhalili et al. [6, 9]. In contrast, others reported post decementation as the major failure mode [8, 27] and explained that, when overloading occurred, the stress would concentrate on the cement between post and dentin, resulting in decementation of the post. In this study, consistent with the FEA analysis, root fracture in the cervical third was also the predominant failure mode of Groups GFR-PEEK and CFR-PEEK, in which the rates of irreparable failure (10% and 20%) were higher than that of PEEK (0%).

CoCr post-and-cores showed the highest stress value and stress concentration in the middle third of the post in the FEA. This could be attributed to the mismatch in elastic modulus between post material (200 GPa) and root dentin (18.6 GPa), and the flexural strength of CoCr (650 MPa) being much higher than that of dentin (212.9 MPa). When the post was loaded, a micro-crack slowly grew at the interfaces of post-cement-dentin; subsequently, the post loosened and acted as a wedge, transferring stress to the less rigid dentine and thus fracturing the root [29, 30]. Group CoCr exhibited the highest static failure load (532.78 ± 40.35 N) in this study, which was much higher than that of Group PEEK (372.03 ± 66.96 N). This was in accordance with the findings in previous studies by Teixeira et al. and Pourkhalili et al., who used NrCr post-and-cores instead of CoCr post-and-cores [8, 9]. In Group CoCr, which exhibited the highest elastic modulus, irreparable failure was observed in most of the specimens, at a rate significantly higher than that of Group PEEK. These findings are consistent with previous studies showing that a substantial proportion of cast metal post-and-core failure was related to catastrophic failure, including root fracture in the middle third, apical third, and vertical root fracture [31–33].

Polymer-infiltrated ceramic (The BRILLIANT Crios; Coltene) comprises 70.7% nano-ceramic (by weight) and 29.3% resin matrix-infiltrated material (by weight), thereby combining the properties of ceramic and composite materials. In addition to the esthetic properties, the mechanical properties of PIC are improved by incorporating ceramic filler [34, 35]. PIC has similar elastic modulus (10.3 GPa) and flexural strength (262 MPa) to dentin, making it suitable for post-and-core restoration. No significant difference was found between Group PIC and the three PEEK groups in terms of stress concentration in the FEA analysis and failure mode in the practical test. Similar results were obtained in other studies [36, 37], which indicated that the abundance of nano-ceramic and the homogeneity of the CAD/CAM blocks would improve the stress distribution. The SFL of Group PIC was higher than those of Groups PEEK and QFRC. Meanwhile, there was no significant difference in this regard among Groups PIC, GFR-PEEK, and CFR-PEEK. A previous study reported that PEEK post-and-cores showed the highest failure load, following by PIC (Vita Enamic, VITA Zahnfabrik) comprising 86% feldspathic ceramic and FRC [6]. Meanwhile, in another study, the failure load of PEEK post-and-cores was comparable to that of post-and-cores of PIC (Lava Ultimate, 3 M) comprising 80% nano-ceramic and FRC [8], which is consistent with the findings of another study by Saisho et al. [11]. These conflicting results may have resulted from the characteristics of the material itself and the methodology used for test, but similar mechanical behavior was evident in those studies. The elastic modulus of PIC is a little lower than that of dentin; hence, a better stress distribution was generated in post-and-cores, reducing the incidence of irreparable failure (10%) compared with that in Group CoCr (80%).

The QFRC post used (MACRO-LOCK®POST ILLUSION®X-RO®; RTD) in this study consists of 80% quartz fiber and 20% epoxy resin. Although the elastic modulus of QFRC (32.1 GPa) is lower than that of CoCr (200 GPa), it is still higher than that of dentin (18.6 GPa) and the three PEEK materials. The QFRC post-and-core showed a similar stress distribution but higher stress concentration than the three PEEK post-and-cores in the FEA, which is also favorable by Hallak et al. [38]. In this study, the stress concentration of the cement layer p in Group QFRC was much higher than in the other groups; subsequently, post decementation inevitably occurred in the restoration of QFRC, which is consistent with previous studies [39–41]. However, when compared with metal posts, the stress distribution of QFRC posts was improved, causing a decrease in the rate of irreparable failure via the relief of impressive stress [42], which was further confirmed in an in vitro study [36]. In terms of the SFL, no significant difference was found between Groups PEEK and QFRC, both of which were lower than those in the other groups. Similar results were obtained in several previous studies that used other fiber-reinforced composite posts [27, 28], while in other studies the opposite result was obtained [6, 9]. In Group QFRC, most of the specimens failed via root fractures in the cervical third of the tooth, which was more favorable than for Group CoCr but similar to the findings for Group PEEK. This matches the results of previous studies [9, 27].

PEEK post-and-cores have been shown to exhibit fatigue resistance under the conventional cyclic loading test under 50 N loading [10, 11]. However, a long time is required to fracture teeth in a laboratory setting under the conventional cycling mode. Therefore, the stepped-load cyclic fatigue test was applied in this study to limit the total testing time and to assess the fatigue resistance of post-and-cores under high loads from 100 to 1000 N [18, 43–46]. The fatigue loading began from a load amplitude of 100 N and increased to 1000 N. To simulate the chewing cycle, sinusoidal load cycles were adopted at a frequency of 5 Hz and the minimum load was equal to 10% of the maximum load [47]. In this study, the groups with PEEK and its fiber-reinforced composites exhibited similar survival rates to the CoCr group under high fatigue loading, which were higher than those of the other groups. Moreover, the values of fatigue failure loads were lower than their corresponding static failure loads because the intrinsic strength of the materials decreased under the cycling load [48], which is consistent with the findings reported by Gontijo et al. [10].

The results of the present study appear promising, but this study has a few limitations that should be mentioned. First, despite the teeth were selected in line with the inclusion criteria and were preferred in accordance with post sizes, the various canal forms and posts may have affected the homogeneity of the thickness of cement between the canal wall and the post. Second, the experiments described here, whether static loading test or fatigue loading test, were conducted in vitro. Randomized clinical trials on endodontically treated teeth restored with PEEK post-and-cores should be performed to prove the reliability of the obtained results. Additionally, more studies should be performed to evaluate the performance of PEEK, GFR-PEEK, and CFR-PEEK post-and-cores under conditions where different amounts of the residual root remain.

Conclusion

1. CoCr post-and-core showed the highest static and fatigue failure load, accompanied with irreparable failure mode. Customized PEEK, GFR-PEEK, and CFR-PEEK post-and-cores exhibited not only similar biomechanical performance but also a more favorable failure mode compared with CoCr post-and-cores.
2. Lower stress concentration and more favorable stress distribution were found in residual roots when restored with customized PEEK, GFR-PEEK, and CFR-PEEK post-and-cores.
3. High survival rates were observed for post-and-cores of PEEK and its composites under high loading amplitude and a large number of cycles.

The findings of this study showed that customized post-and-cores manufactured with PEEK and its fiber-reinforced composites exhibited superior biomechanical performance, making them potential alternatives for the restoration of massive tooth defects.

Abbreviations

CAD Computer Aided Design
CAM Computer Aided Manufacture
CEJ Cemento-enamel Junction
CFF Cycles for failure
CFR-PEEK Carbon fiber-reinforced PEEK
CoCr Cobalt Chromium
FFL Fatigue failure load
GFR-PEEK Glass fiber-reinforced PEEK
PEEK Polyetheretherketone
PIC Polymer infiltrated ceramic
QFRC Quartz-fiber-reinforced composite
SFL Static failure load
SPSS Statistical Product and Service Solutions

Acknowledgements

Not applicable.

Author contributions

Biyao Wang: Writing - original draft, Methodology, Investigation, Data curation, Formal analysis. Minghao Huang: Methodology, Investigation. Kaige Zhang: Methodology, Investigation. Yan Xu: Data curation, Formal analysis. Xinwen Zhang: Data curation, Formal analysis. Liye Shi: Writing - review & editing, Project administration. Xu Yan: Conceptualization, Supervision, Funding acquisition, Resources.

Funding

This work was supported by the Provincial Nature Science Foundation of Liaoning (No. 2021-YGJC-25 to X.Y.) and the Municipal Science and Technology Project of Shenyang (No. 20-205-4-079 to X.Y.).

Data availability

Data is not publicly available but anonymized sets of data and replication files are available from the authors on request.

Declarations

Ethics approval and consent to participate

This study was conducted in accordance with the Declaration of Helsinki, and the protocol was approved by the Medical Ethics Committee of the Hospital of Stomatology of China Medical University (2022; No. 7).

Consent for publication

Not applicable.

Competing interests

The authors declare no competing interests.

Author details

[1]The VIP Department, School and Hospital of Stomatology, Liaoning Provincial Key Laboratory of Oral Diseases, China Medical University, No.117 North street Nanjing Road, Shenyang 110002, China
[2]Department of Oral Implantology, School and Hospital of Stomatology, Liaoning Provincial Key Laboratory of Oral Diseases, China Medical University, Shenyang, China
[3]The Comprehensive Department, Shenyang Stomatological Hospital, Shenyang, China
[4]Laboratory Animal Centre, School and Hospital of Stomatology, China Medical University, Shenyang, China
[5]Geriatric Medicine Department, The First Affiliated Hospital, China Medical University, Shenyang, China

Received: 15 July 2024 / Accepted: 1 May 2025
Published online: 10 May 2025

References

1. Lee KS, Shin JH, Kim JE, Kim JH, Lee WC, Shin SW, Lee JY. Biomechanical evaluation of a tooth restored with high performance polymer PEKK post-core system: a 3D finite element analysis. Biomed Res Int. 2017;2017:1373127.
2. Machado J, Almeida P, Fernandes S, Marques A, Vaz M. Currently used systems of dental posts for endodontic treatment. Procedia Struct Integr. 2017;5:27–33.

3. Spazzin AO, Galafassi D, de Meira-Júnior AD, Braz R, Garbin CA. Influence of post and resin cement on stress distribution of maxillary central incisors restored with direct resin composite. Oper Dent. 2009;34(2):223–9.
4. Meira JB, Espósito CO, Quitero MF, Poiate IA, Pfeifer CS, Tanaka CB, Ballester RY. Elastic modulus of posts and the risk of root fracture. Dent Traumatol. 2009;25(4):394–8.
5. Junqueira RB, de Carvalho RF, Marinho CC, Valera MC, Carvalho CAT. Influence of glass fibre post length and remaining dentine thickness on the fracture resistance of root filled teeth. Int Endod J. 2017;50(6):569–77.
6. Haralur SB. Fracture resistance of endodontically treated teeth restored with various esthetic posts. Technol Health Care. 2021;29(2):243–52.
7. Wang B, Huang M, Dang P, Xie J, Zhang X, Yan X. PEEK in fixed dental prostheses: application and adhesion improvement. Polymers. 2022;14(12):2323.
8. Teixeira KN, Duque TM, Maia HP, Gonçalves T. Fracture resistance and failure mode of custom-made post-and-cores of polyetheretherketone and nano-ceramic composite. Oper Dent. 2020;45(5):506–15.
9. Pourkhalili H, Maleki D. Fracture resistance of polyetheretherketone, Ni-Cr, and fiberglass postcore systems: an in vitro study. Dent Res J (Isfahan). 2022;19:20.
10. Gontijo IG, Ferretti MA, Caldas RA, Pecorari VGA, França FMG, Oliveira LKN, Aguiar FHB. Biomechanical behavior of weakened roots restored with custom-made post-and-cores of glass fiber and polyetheretherketone. J Prosthodont. 2022;32(9):807–14
11. Saisho H, Marcolina G, Perucelli F, Goulart da Costa R, Machado de Souza E, Rached RN. Fracture strength, pull-out bond strength, and volume of luting agent of tooth-colored CAD-CAM post-and-cores. J Prosthet Dent. 2023;129(4):599–606.
12. Tanaka R, Yamaguchi S, Takahashi Y, Imazato S, Hayashi M. Mechanical behavior of endodontically treated teeth: a three-dimensional finite element analysis using displacement vector. J Prosthodont. 2023;34(3):281–9
13. Huang M, Wang B, Zhang K, Yan X, Chen Z, Zhang X. Comparative analysis of stress distribution in residual roots with different canal morphologies: evaluating CAD/CAM glass fiber and other post-core materials. BMC Oral Health. 2024;24(1):337.
14. Ding X, Li J, Zhang X, Yan X. Effects of 3 different residual root treatments after post-and-core restoration: an in vitro fracture resistance experiment and finite element analysis. J Prosthet Dent. 2020;124(4):e485481–485410.
15. Nahar R, Mishra SK, Chowdhary R. Evaluation of stress distribution in an endodontically treated tooth restored with four different post systems and two different crowns- a finite element analysis. J Oral Biology Craniofac Res. 2020;10(4):719–26.
16. Stawarczyk B, Jordan P, Schmidlin PR, Roos M, Eichberger M, Gernet W, Keul C. PEEK surface treatment effects on tensile bond strength to veneering resins. J Prosthet Dent. 2014;112(5):1278–88.
17. Gale MS, Darvell BW. Thermal cycling procedures for laboratory testing of dental restorations. J Dent. 1999;27(2):89–99.
18. Borba M, Cesar PF, Griggs JA, Della Bona A. Step-stress analysis for predicting dental ceramic reliability. Dent Mater. 2013;29(8):913–8.
19. Suzaki N, Yamaguchi S, Nambu E, Tanaka R, Imazato S, Hayashi M. Fabricated CAD/CAM post-core using glass fiber-reinforced resin shows innovative potential in restoring pulpless teeth. Materials (Basel, Switzerland). 2021;14(20).
20. Sturm R, Prates Soares A, Sterzenbach G, Bitter K. Interface analysis after fatigue loading of adhesively luted bundled fiber posts to human root canal dentin. J Mech Behav Biomed Mater. 2021;119:104385.
21. Attia MA, Shokry TE, Abdel-Aziz M. Effect of different surface treatments on the bond strength of milled polyetheretherketone posts. J Prosthet Dent. 2021;127(6):866–74
22. Monteiro LC, Pecorari VGA, Gontijo IG, Marchi GM, Lima D, Aguiar FHB. PEEK and fiberglass intra-radicular posts: influence of resin cement and mechanical cycling on push-out bond strength. Clin Oral Investig. 2022;26(12):6907–16
23. Penteado MM, de Andrade GS, Araujo RM, Borges ALS, Valandro LF, Pereira GKR, da Silva JMF. Fatigue survival of endodontically treated teeth restored with different fiber-reinforced composite resin post strategies versus universal 2-piece fiber post system: an in vitro study. J Prosthet Dent. 2021;129(3):456–63
24. Caglar I, Ates SM, Yesil Duymus Z. An in vitro evaluation of the effect of various adhesives and surface treatments on bond strength of resin cement to polyetheretherketone. J Prosthodont. 2019;28(1):e342–9.
25. Yu H, Feng Z, Wang L, Mihcin S, Kang J, Bai S, Zhao Y. Finite element study of PEEK materials applied in post-retained restorations. Polymers. 2022;14(16).
26. Steiner M, Mitsias ME, Ludwig K, Kern M. In vitro evaluation of a mechanical testing chewing simulator. Dent Mater. 2009;25(4):494–9.
27. Özarslan M, Büyükkaplan U, Özarslan MM. Comparison of the fracture strength of endodontically treated teeth restored with polyether ether ketone, zirconia and glass-fibre post-core systems. Int J Clin Pract. 2021;75(9):e14440.
28. Sugano K, Komada W, Okada D, Miura H. Evaluation of composite resin core with prefabricated polyetheretherketone post on fracture resistance in the case of flared root canals. Dent Mater J. 2020;39(6):924–32.
29. da Silva NR, Raposo LH, Versluis A, Fernandes-Neto AJ, Soares CJ. The effect of post, core, crown type, and ferrule presence on the biomechanical behavior of endodontically treated bovine anterior teeth. J Prosthet Dent. 2010;104(5):306–17.
30. Barcellos RR, Correia DP, Farina AP, Mesquita MF, Ferraz CC, Cecchin D. Fracture resistance of endodontically treated teeth restored with intra-radicular post: the effects of post system and dentine thickness. J Biomech. 2013;46(15):2572–7.
31. Palepwad AB, Kulkarni RS. In vitro fracture resistance of zirconia, glass-fiber, and cast metal posts with different lengths. J Indian Prosthodont Soc. 2020;20(2):202–7.
32. Martins MD, Junqueira RB, de Carvalho RF, Lacerda M, Faé DS, Lemos CAA. Is a fiber post better than a metal post for the restoration of endodontically treated teeth? A systematic review and meta-analysis. J Dent. 2021;112:103750.
33. Tsintsadze N, Margvelashvili-Malament M, Natto ZS, Ferrari M. Comparing survival rates of endodontically treated teeth restored either with glass-fiber-reinforced or metal posts: a systematic review and meta-analyses. J Prosthet Dent. 2022;131(4):567–78
34. Lauvahutanon S, Takahashi H, Shiozawa M, Iwasaki N, Asakawa Y, Oki M, Finger WJ, Arksornnukit M. Mechanical properties of composite resin blocks for CAD/CAM. Dent Mater J. 2014;33(5):705–10.
35. Leung BT, Tsoi JK, Matinlinna JP, Pow EH. Comparison of mechanical properties of three machinable ceramics with an experimental fluorophlogopite glass ceramic. J Prosthet Dent. 2015;114(3):440–6.
36. Falcão Spina DR, Goulart da Costa R, Farias IC, da Cunha LG, Ritter AV, Gonzaga CC, Correr GM. CAD/CAM post-and-core using different esthetic materials: fracture resistance and bond strengths. Am J Dent. 2017;30(6):299–304.
37. Sary SB, Samah MS, Walid AA. Effect of restoration technique on resistance to fracture of endodontically treated anterior teeth with flared root canals. J Biomedical Res. 2019;33(2):131–8.
38. Hallak AG, Caldas RA, Silva ID, Miranda ME, Brandt WC, Vitti RP. Stress distribution in restorations with glass fiber and polyetheretherketone intraradicular posts: an in silico analysis. Dent Mater J. 2022.41(3): 376–81
39. Song CH, Choi JW, Jeon YC, Jeong CM, Lee SH, Kang ES, Yun MJ, Huh JB. Comparison of the microtensile bond strength of a polyetherketoneketone (PEKK) tooth post cemented with various surface treatments and various resin cements. Mater (Basel Switzerland). 2018;11(6).
40. Bru E, Forner L, Llena C, Almenar A. Fibre post behaviour prediction factors. A review of the literature. J Clin Exp Dent. 2013;5(3):e150–153.
41. Maroulakos G, Nagy WW, Kontogiorgos ED. Fracture resistance of compromised endodontically treated teeth restored with bonded post and cores: an in vitro study. J Prosthet Dent. 2015;114(3):390–7.
42. Pegoretti A, Fambri L, Zappini G, Bianchetti M. Finite element analysis of a glass fibre reinforced composite endodontic post. Biomaterials. 2002;23(13):2667–82.
43. Silva N, Bonfante EA, Rafferty BT, Zavanelli RA, Rekow ED, Thompson VP, Coelho PG. Modified Y-TZP core design improves all-ceramic crown reliability. J Dent Res. 2011;90(1):104–8.
44. Coelho PG, Bonfante EA, Silva NRF, Rekow ED, Thompson VP. Laboratory simulation of Y-TZP all-ceramic crown clinical failures. J Dent Res. 2009;88(4):382–6.
45. Venturini AB, Prochnow C, Pereira GKR, Segala RD, Kleuerlaan CJ, Valandro LF. Fatigue performance of adhesively cemented glass-, hybrid- and resin-ceramic materials for CAD/CAM monolithic restorations. Dent Mater. 2019;35(4):534–42.
46. de Carvalho MA, Lazari-Carvalho PC, Del Bel Cury AA, Magne P. Fatigue and failure analysis of restored endodontically treated maxillary incisors without a dowel or ferrule. J Prosthet Dent. 2022;131(2):241–50
47. Kruzic JJ, Nalla RK, Kinney JH, Ritchie RO. Mechanistic aspects of in vitro fatigue-crack growth in dentin. Biomaterials. 2005;26(10):1195–204.

48. Yahyazadehfar M, Mutluay MM, Majd H, Ryou H, Arola D. Fatigue of the resin-enamel bonded interface and the mechanisms of failure. J Mech Behav Biomed Mater. 2013;21:121–32.

Publisher's note